Twenty-Fifth Symposium (International) on Combustion/The Combustion Institute, 1994/pp. 759–766

NEW RESULTS ON MOIST CO OXIDATION: HIGH PRESSURE, HIGH TEMPERATURE EXPERIMENTS AND COMPREHENSIVE KINETIC MODELING

TAE J. KIM, RICHARD A. YETTER AND FREDERICK L. DRYER
Department of Mechanical and Aerospace Engineering
Princeton University
Princeton, New Jersey 08544, USA

The kinetics of moist carbon monoxide oxidation have been studied experimentally for pressures from 1 to 9.6 atm, temperatures from 960 to 1200 K, and equivalence ratios from 0.33 to 2.1. New data were used in combination with prior flow reactor, shock tube, and static reactor data to develop a revised comprehensive reaction mechanism for the $CO/H_2O/O_2$ system. In particular, the new data span the explosion limit behavior of the system and place significantly increased emphasis on the kinetics involving the hydroperoxyl radical. Revisions of the rates recommended in an earlier comprehensive mechanism are needed in order to reproduce experimental observations. While six reaction recommendations were modified, the most important were the kinetic parameters for $H_2O + O = OH + OH$ and $HO_2 + OH = H_2O + O_2$.

Experimentally, the second limit for this reaction system was determined at much higher pressures than previously studied. Near the limit, an increase in pressure results in a two order of magnitude decrease in the oxidation rate. Away from the limit, the pressure dependence of the rate is similar in both the nonexplosive and explosive regimes. In the nonexplosive regime, the kinetics are straight chain in nature and governed by the reactions $H + O_2 + M = HO_2 + M$, $CO + HO_2 = CO_2 + OH$, and $CO + OH = CO_2 + H$. The overall temperature dependence of the oxidation is very large (77 kcal/mol). In the explosive regime, chain-branching phenomena dominate and are controlled by the reactions $H + O_2 = OH + O$, $CO + OH = CO_2 + H$, and $O + H_2O = OH + OH$. The overall temperature dependence of the oxidation is significantly lower (40 kcal/mol). The sensitivity of the reaction rate to moisture saturates at much lower moisture concentration in the nonexplosive regime. At high pressures (>25 atm), the oxidation of CO through $CO + OH = CO_2 + H$ and $CO + HO_2 = CO_2 + OH$ is numerically predicted to approach a limiting ratio of one-half.

Introduction

Characterization of moist carbon monoxide oxidation, in particular, its hydroperoxyl reaction chemistry, has typically involved studies in static reactors at subatmospheric pressure and below 800 K. In earlier work in which we developed and validated a comprehensive reaction mechanism for CO oxidation, we stated that the reactions involving HO_2 and H_2O_2 were most likely going to require further consideration. Many of the reactions involving these species involve an association complex at low temperatures and a direct abstraction reaction at high temperatures. These competing channels result in an overall rate constant behavior with a negative activation energy at low temperatures and a positive activation energy at high temperatures. For example, this type of behavior has been recently observed for reactions of $HO_2 + HO_2 = H_2O_2 + O_2$ [1] and $H_2O_2 + OH = H_2O + HO_2$ [2,3]. Testing reaction mechanisms against static reactor experimental results is necessarily insensitive to the high-temperature characterization of such reactions, and these reactions are essential for modeling conventional high-pressure combustion environments. This paper presents new experimental data on the moist carbon monoxide reaction at appropriate pressures and temperatures to increase the sensitivity of observations to the abstraction channels for some of these reactions. The experimental data are then utilized to revise and extend the comprehensive reaction mechanism published earlier [4].

Parametric studies of the $CO/H_2O/O_2$ system are performed in a flow reactor for pressures from 1 to 9.6 atm, temperatures from 960 to 1200 K, and for equivalence ratios from 0.33 to 2.1. The present data span both the explosive and nonexplosive kinetic regimes as well as the boundary between them. Figure 1 displays prior data on the moist CO explosion limits [5–8] in comparison to the conditions reported here.

Experiment

Experiments have been conducted in a variable temperature ($600 < T < 1200$ K), variable pressure

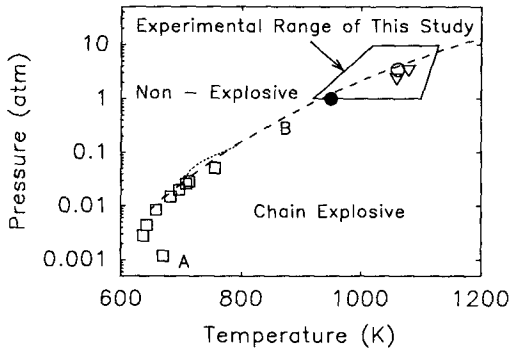

FIG. 1. The moist CO/O_2 explosion limits that separate explosive from nonexplosive chemistry. The first and second limits are given by A and B, respectively. Previous explosion limits data [6–8] are also shown. The third body, M, is N_2. The figure key is as follows: ○ 0.65% H_2O, φ = 1, this study; ▽ 0.65% H_2O, φ = 0.33, this study; ● 1.04% H_2O, φ = 1 [8]; □ 1.0% H_2, φ = 1 [6]; ····· 20% H_2, φ = 1 [7]; ---- [M] = $2k_1/k_9$.

($1 < P < 20$ atm) flow reactor [9–13] with residence times ranging from 10 ms to 2 s. A schematic diagram of the variable pressure flow reactor is given in Fig. 2. Carbon monoxide and water vapor, along with about 10% of the total nitrogen flow, are injected into the carrier and oxidizer stream at the mixer, located just prior to a conical silica foam diffuser. The mixer is jet stirred and has a nominal turnover time of about 0.5% of the total test time. A combined ferrous alloy/tungsten electrical resistance heater is used to heat the carrier gas upstream of the test section. The flow reactor is operated as a steady, isobaric flow device, and the time from mixing to sample position is varied by moving the mixer/diffuser assembly along the quartz test tube.

The pressure vessel is designed to enclose not only the reactor section (the reactor duct heaters and insulation) but also the positioning mechanism and fuel/water vapor injection probe, which axially locates the fuel/carrier mixing section relative to the sampling location. The reaction duct itself is quartz, 173-cm long with a 10.16-cm inside diameter. The entire quartz tube is surrounded by electric heaters, which maintain the walls at the initial gas temperature. This creates a nearly adiabatic system since chemical energy release in this highly dilute mixture results in small gas/wall temperature gradients.

In order to translate flow reactor position into reaction time, the mean velocity distribution along the centerline is measured under cold flow conditions using pitot-static probe techniques. These measurements are related to experimental conditions through Reynolds number correlations.

A hot water-cooled, stainless steel sample probe is mounted in the reactor end flange and is used to continuously extract and convectively quench a small portion of the reacting gases. From the probe, the gas sample flow is sent to a Fourier transform infrared (FTIR), a continuous electrochemical analyzer for O_2, and continuous nondispersive infrared (NDIR) analyzers for CO and CO_2. The sample temperature is measured with a silica-coated Pt/Pt-13% Rh thermocouple. Further details concerning these experiments can be found in Ref. 11.

Reaction Mechanism

The reaction mechanism resulting from this study is given in Table 1. Reverse rate constants are derived from the listed forward rates and equilibrium constants calculated from the thermochemical data presented in Table 2 [14,15]. The present reaction mechanism is a revision of the comprehensive reaction mechanism of Yetter et al. [4]. In another recent paper [12], mixtures of hydrogen/oxygen were studied for pressures of $1 < P < 15.7$ atm and temperatures of $850 < T < 1010$ K. The HO_2/H_2O_2 rate expressions utilized earlier [4] had been critically evaluated for temperatures below 800 K. For encompassing these new experiments [12] and the ones reported here, reactions involving adducts and pressure dependencies of recombination reactions

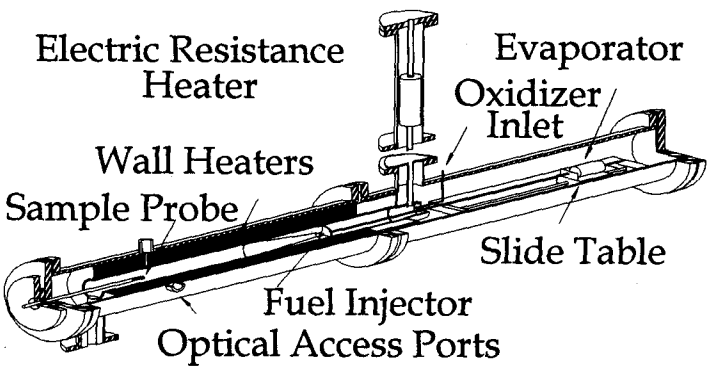

FIG. 2. A cutaway view of the variable pressure flow reactor.

TABLE 1
$CO/H_2/O_2$ reaction mechanism
(units are cm^3 mol s kcal K; $k = AT^n \exp(-E_a/RT)$ unless specified)

	$\log(A_f)$	n_f	$E_{a,f}$	UF[b]	T[a]	Ref.
H_2-O_2 chain reactions						
1. $H + O_2 = O + OH$	14.28	0.0	16.44	2	962–2,577	37
2. $O + H_2 = H + OH$	4.71	2.67	6.29	1.5	297–2,495	38
3. $OH + H_2 = H + H_2O$	8.33	1.51	3.43	1.5	250–2,581	39
4. $O + H_2O = OH + OH$	6.47	2.02	13.40	2.5	250–2,000	19
H_2-O_2 dissociation/recombination reactions						
5. $H_2 + M = H + H + M$	19.66	−1.40	104.38	3	600–2,000	18[c]
$H_2 + Ar = H + H + Ar$	18.77	−1.10	104.38	2	600–5,000	18
6. $O + O + M = O_2 + M$	15.79	−0.50	0.00	1.3	2,000–10,000	18
$O + O + Ar = O_2 + Ar$	13.28	0.0	−1.79	1.3	2,000–4,000	18
7. $O + H + M = OH + M$	18.67	−1.0	0.00	10		18
8. $H + OH + M = H_2O + M$	22.35	−2.0	0.00	2	1,000–3,000	18
$H + OH + Ar = H_2O + Ar$	21.92	−2.0	0.00	2	1,000–3,000	18
Formation and Consumption of HO_2						
9. $H + O_2 + M = HO_2 + M$	19.79	−1.42	0.00	3	200–2,000	21[d]
$H + O_2 + Ar = HO_2 + Ar$	15.18	0.0	−1.00	2	300–2,000	40
$H + O_2 = HO_2$	13.65	0.0	0.00	1.3	298	22
10. $HO_2 + H = H_2 + O_2$	13.82	0.0	2.13	2	298–773	18
11. $HO_2 + H = OH + OH$	14.23	0.0	0.87	2	298–773	18
12. $HO_2 + O = OH + O_2$	13.24	0.0	−0.40	1.2	200–400	18
13. $HO_2 + OH = H_2O + O_2$	16.28	−1.00	0.00	2	254–1,050	see text
Formation and consumption of H_2O_2						
14. $HO_2 + HO_2 = H_2O_2 + O_2$	14.62	0.0	11.98			
	11.11	0.0	−1.629	3	650–800	1[e]
15. $H_2O_2 + M = OH + OH + M$	17.08	0.0	45.50	2	700–1,500	41[d]
$H_2O_2 + Ar = OH + OH + Ar$	16.28	0.0	43.00	2	700–1,500	23
$H_2O_2 = OH + OH$	14.47	0.0	48.40	2	1,000–1,500	23
16. $H_2O_2 + H = H_2O + OH$	13.00	0.0	3.59	3	283–800	41
17. $H_2O_2 + H = H_2 + HO_2$	13.68	0.0	7.95	5	283–800	18
18. $H_2O_2 + O = OH + HO_2$	6.98	2.0	3.97	3	250–800	18
19. $H_2O_2 + OH = H_2O + HO_2$	12.00	0.0	0.00			
	14.76	0.0	9.56	2	250–1,250	3[e]
Oxidation of CO						
20. $CO + O + M = CO_2 + M$	13.40	0.0	−4.54	4	1,000–3,000	41
$CO + O + Ar = CO_2 + Ar$	13.34	0.0	−4.54	4	1,000–3,000	41
21. $CO + O_2 = CO_2 + O$	12.40	0.0	47.69	2	1,500–3,000	18
22. $CO + OH = CO_2 + H$	7.176	1.3	−0.765	1.5	250–2,500	42
23. $CO + HO_2 = CO_2 + OH$	13.78	0.0	22.95	3	700–1,000	43
Formation and consumption of HCO						
24. $HCO + M = H + CO + M$	17.27	−1.0	17.00	5	637–832	44
$HCO + Ar = H + CO + Ar$	17.27	−1.0	17.00	5	637–832	44
25. $HCO + O_2 = CO + HO_2$	12.88	0.0	0.41	5	295–713	45
26. $HCO + H = CO + H_2$	13.86	0.0	0.00	2	296–418	46
27. $HCO + O = CO + OH$	13.48	0.0	0.00	3		18
28. $HCO + OH = CO + H_2O$	13.48	0.0	0.00	3		18

[a] T is the temperature range over which the rate constant parameters are evaluated.
[b] UF is an estimated uncertainty factor for the specified T range; $+\Delta k/k = UF - 1$ and $-\Delta k/k = UF^{-1} - 1$.
[c] Efficiency factors for pressure-dependent reactions with an unspecified collision partner are $\varepsilon_{N_2} = 1.0$, $\varepsilon_{H_2} = 2.5$; $\varepsilon_{H_2O} = 12$, $\varepsilon_{CO} = 1.9$; $\varepsilon_{CO_2} = 3.8$. All other species have efficiencies equal to unity.
[d] k_{uni} is given for reaction 15 as a Troe fit [20] with $F_c = 0.5$ [23] and for reaction 9 as a Lindemann fit [20].
[e] k for reactions 14 and 19 are the sums of two rate constant expressions.

TABLE 2
Thermochemical constants at 298.15 K (units are cal mol^{-1} deg^{-1} for C_p and S and kcal mol^{-1} for ΔH_f

Species	ΔH_f	S	C_p
H	52.101 ± 0.001	27.416 ± 0.004	4.97[a]
O	59.55 ± 0.024	38.492 ± 0.005	5.24
OH	9.318 ± 0.29	43.905 ± 0.01	7.17
H_2	0	31.232 ± 0.008	6.89
O_2	0	49.106 ± 0.008	7.02
H_2O	−57.795 ± 0.01	45.13 ± 0.01	8.03
HO_2	3.0 ± 2.0	54.76 ± 0.02	8.34[b]
H_2O_2	−32.53	55.68	10.30
CO	−26.42 ± 0.04	47.24 ± 0.01	6.96
CO_2	−94.05 ± 0.012	51.10 ± 0.03	8.87
HCO	10.40 ± 1.9	53.69 ± 0.01	8.27
N_2	0	45.793 ± 0.005	6.97
Ar	0	37.007 ± 0.001	4.97

[a]All data are from Ref. 14 except $\Delta H_f(HO_2)$. Polynominal fit coefficients from Ref. 16.

[b]$\Delta H_f(HO_2)$, from Ref. 15. For HO_2, polynominal fit coefficients are derived from Ref.17.

needed to be reconsidered. The rate constant expressions for reactions (4), (9), (13) through (15), and (19) in Table 1 have been modified in response to recently reported elementary kinetic data and the present mechanistic studies.

The change in k_4 is predicated on the recent measurements of Sutherland et al. [19]. Falloff for reaction (9) is expressed in terms of a Lindemann fit [20] using the Slack [21] low-pressure expression and the Cobos et al. high-pressure data [22]. Falloff for reaction (15) is expressed in a Troe fit [20] using the data of Brouwer et al. [23]. The rate constants, k_{14} and k_{19}, are from Hippler and coworkers [1,3] and are expressed as the sum of two exponentials.

The rate constant k_{13} is based on the low-temperature data ($254 < T < 382$ K) of Keyser [24] and recent high-temperature data (1050 K) of Hippler and Troe [3,25]. Figure 3 is an Arrhenius plot of these data and other kinetic studies. The data of Keyser [24] is the favored low-temperature rate recommended by two recent critical reviews [20,26]. The high-temperature data exhibit considerably more scatter. In the original mechanism, reaction (13) was from the critical review of Tsang and Hampson [18], which was based upon the low-temperature data of Sridharan et al. [31]. Roesler et al. [33] have shown that for fuel lean $CO/H_2O/O_2$ mixtures at 1000 K and 1 atm, where reaction (13) is among the most sensitive but with the largest uncertainty, the Tsang and Hampson expression [18] underpredicted the necessary amount of termination. The measurements of

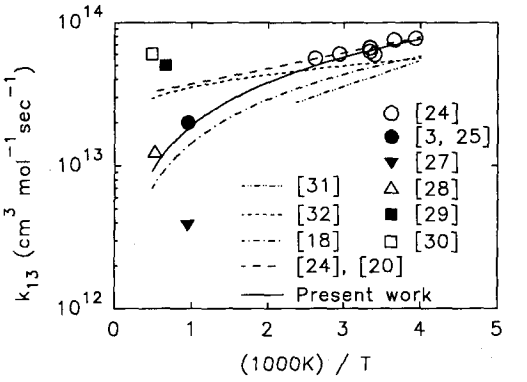

FIG. 3. An Arrhenius plot for the $HO_2 + OH = H_2O + O_2$ reaction. Recent data acquired by Keyser [24] and Hippler and Troe [3,25] were used to generate the curve fit of this recommendation given by $k_{13} = 1.9 \times 10^{16} T^{-1}$. Also shown are the recommended fits of Tsang and Hampson [18], Keyser [24], Sridharan et al. [31], and Gonzalez et al. [32].

Hippler and Troe [3,25] are in agreement with the observations of Roesler et al. [33]. Using the data of Keyser [24] and Hippler and Troe [3,25], a new rate constant expression for k_{13} between 298 and 1050 K is reported here (Table 1).

Finally, Chaperon efficiencies for recombination/dissociation reactions were treated in the same manner as in our earlier work [4]. The reaction parameters for CO + O + M remain ill-defined, and additional elementary studies are needed for this reaction [4].

After conversion of the spatial flow reactor data into reaction time using velocity data, the kinetic data were modeled assuming a zero-dimensional, isobaric, adiabatic, homogenous system. The kinetic and associated sensitivity equations were solved using SENKIN [47]. For modeling and data comparisons, model predictions were time shifted to match the point of 50% fuel consumption [8].

Results and Discussion

In Fig. 4, experimental and calculated profiles of the CO mole fraction X(CO), as a function of residence time, are presented for 1 and 3.46 atm at 1040 K ($\phi = 1$). The symbols are the experimental data, and the lines are model predictions using the refined (solid line) and original (dashed line) mechanisms. At 1 atm, the initial condition of the mixture is within the explosive region, which is below the second limit (see Fig. 1). Here, the predictions of the two mechanisms are virtually identical. As the dilute mixture begins to react at constant pressure, the temperature of the gas rises to a final temperature of 1110 K. At

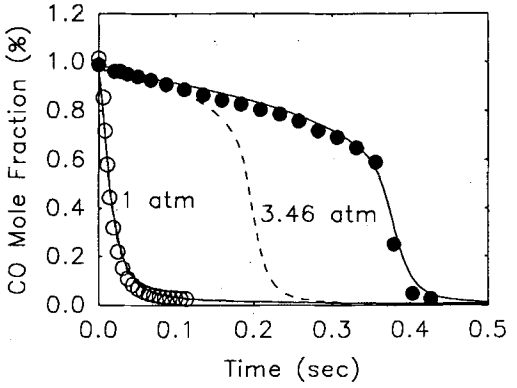

FIG. 4. A comparison of 1 and 3.46 atm data with model predictions using the original mechanism of Yetter et al. [4] ------and the present mechanism————. Initial conditions are an initial temperature of 1040 K, 1.0% CO, 0.5% O_2, 0.65% H_2O, balance N_2. For the 1 atm case, the two model predictions are essentially identical.

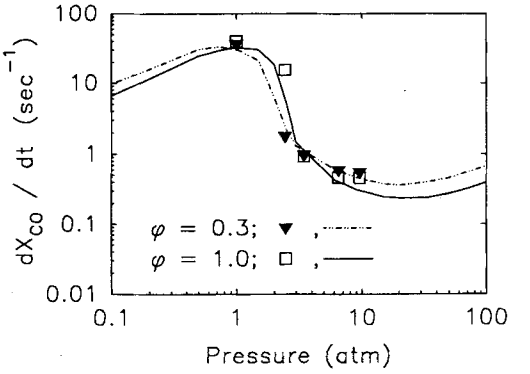

FIG. 5. The effect of pressure on the rate of CO oxidation at 1040 K for equivalence ratios of 1 and 0.333. The oxidation rate is given by the mean slope of dX_{co}/dt between 15 and 65% fuel consumption. Initial mole fractions are 1.0% CO and 0.65% H_2O, balance N_2. Symbols are the experimental data, and lines are the model calculations.

3.46 atm, the initial condition is in the nonexplosive regime, just above the second limit. The CO data exhibit an initial period of slow decay followed by a sudden transition to fast decay. This transition occurs at the temperature of the second limit. Calculations based on the original mechanism cross the second limit at a lower temperature/higher X(CO) than the data, with the resulting reaction times differing by a factor of 2. Predictions using the refined mechanism compare well with the higher-pressure data.

The second explosion limit data for stoichiometric moist CO/O_2 mixtures are shown in Fig. 1 to correlate with $[M] = 2k_1/k_9$, the classical second explosion limit result for stoichiometric H_2/O_2 mixtures. The effect of varying the H_2O concentration at the CO/O_2 second limit has been investigated numerically for a 1.0% CO, 0.5% O_2 mixture at 3.46 atm [11]. As the $X(H_2O)$ approaches zero, the explosion temperature asymptotically increases. For $X(H_2O)$ exceeding 0.0065, increasing $X(H_2O)$ has little effect on the explosion temperature. Thus, the H_2/O_2 submechanism controls the explosion condition in the present experiments and those of Yetter et al. [8]. This result is consistent with earlier theory [34,35].

At the second limit, the effect of varying the equivalence ratio was also studied. As the O_2/CO ratio increases, the explosion condition is shifted to higher temperatures/lower pressures (Fig. 1). This effect results from a change in HO_2 consumption paths from a suppression of H-atom concentrations relative to O and OH [33]. This trend agrees with other data [6] and is also numerically predicted by the revised reaction mechanism [11].

Figure 5 shows how the overall oxidation rate responds to pressure, for a fixed temperature of 1040 K and initial mole fraction of 1% CO and two equivalence ratios (ϕ = 1 and 0.33). As the second explosion limit is crossed, the oxidation rate decreases by approximately two orders of magnitude. However, the dependence of the oxidation rate with respect to pressure is nearly the same in both the explosive and nonexplosive regimes. The oxygen dependence of this reaction at atmospheric pressure has been shown to be a complex function of temperature [33]. At 1040 K (Fig. 5), there is no oxygen dependence. At lower temperatures, oxygen addition inhibits the reaction, while at higher temperatures, oxygen addition accelerates the reaction. Here, we note similar complexities in oxygen dependence due solely to changes in reaction pressure.

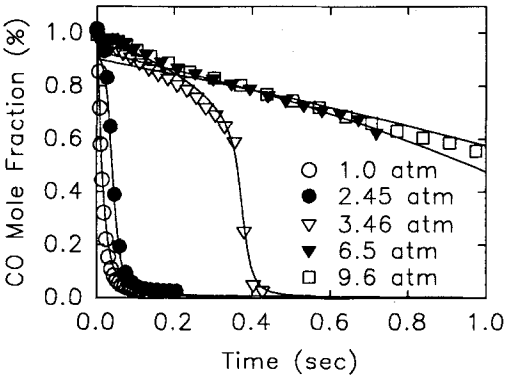

FIG. 6. Detailed comparisons of experimental CO decay profiles (symbols) with modeling predictions based on the refined mechanism (lines). For pressures from 1 to 9.6 atm, the initial mole fractions are 1.0% CO, 0.5% O_2, and 0.65% H_2O, balance N_2. The initial temperature was 1040 K.

Figure 6 presents detailed comparisons of the ex-

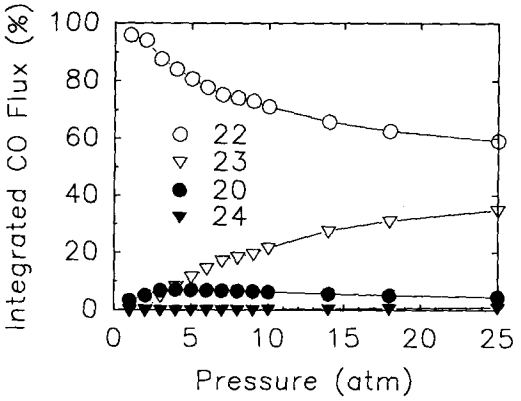

FIG. 7. Numerical calculations of the time-integrated CO flux at 1 atm (open bars) and 9 atm (solid bars) as a function of pressure. Initial conditions are the same as for the previous figure. Reaction numbers correspond to those listed in Table 1.

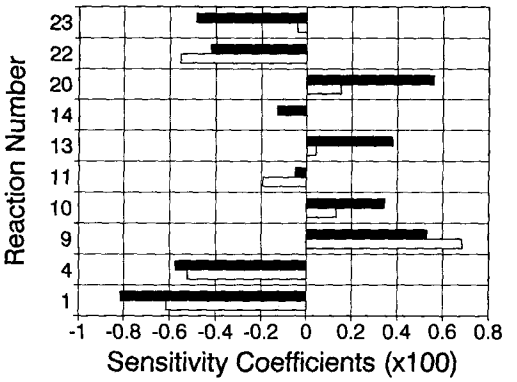

FIG. 8. Sensitivity coefficients given by $(\partial Y_{CO}/\partial \ln k_j)$ at the point of 50% CO consumption for 1 and 9 atm. Y_{CO} is the CO mass fraction and k_j is the jth rate constant. The mixture is the same as in Fig. 6. Reaction numbers correspond to those listed in Table 1.

perimental data with model comparisons for pressures from 1 to 9.6 atm and $\phi = 1$. The inhibiting effect of pressure is clearly seen on the reaction profiles. As pressure is increased, the mechanism changes from explosive chemistry, to transition chemistry, and then to nonexplosive chemistry. Similar agreement between experiment and model is obtained for $\phi = 0.33$ [11].

As the pressure is increased, different reaction sets in the mechanism become important. Numerical calculations showing the effects of increasing pressure on the various CO fluxes are presented in Fig. 7. At atmospheric pressure, the system is explosive and reaction (22) consumes about 95% of the CO. As the pressure is increased, the amount of termination resulting from reaction (9) increases relative to the branching from reaction (2). As a result, the H, O, and OH levels are suppressed relative to the HO_2 levels, and reaction (23) becomes important as a means of converting CO. At 25 atm, reaction (23) consumes over 35% of the CO, while reaction (22) consumes less than 60%. Note that the fluxes of reactions (22) and (23) asymptotically approach one another.

Sensitivity and reaction flux analyses were utilized to identify changes in the reaction mechanism due to pressure (Fig. 8). At atmospheric pressure, the sensitivity coefficients are dominated by those for reactions (2), (9), (22), and (4). The sensitivity coefficients for the other reactions including (10), (11), (20), (23), and (13) are relatively small. In contrast, the sensitivity coefficients for many of these reactions are of comparable magnitude at 9 atm. While the mechanism remains very sensitive to reactions (2) and (9), the system is more sensitive to reactions (23) and (20) than to (22). Furthermore, the sensitivity of the system to reactions (13), (4), and (14) are larger

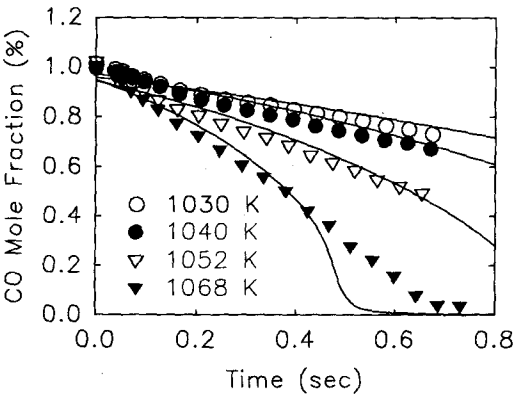

FIG. 9. Comparisons of experimental CO profiles with modeling predictions for initial temperatures from 1030 to 1068 K at 6.5 atm. The mixture is the same as in Fig. 6.

than at atmospheric pressure. From reaction flux analysis, the overall reaction is branched chain in nature at atmospheric pressure and driven by reactions (2), (22), and (4). As pressure is increased, this branched chain sequence is heavily suppressed, and the overall reaction becomes straight chain, driven by reactions (9), (22), and (23). Increasing pressure also slows the oxidation rate because of the increased importance of terminating reactions such as (9), (13), and (20).

Of particular interest is that the experimental system is highly temperature sensitive in the nonexplosive regime. In Fig. 9, the lowest and highest initial temperatures differ by only 38 K, less than a 4% change in initial temperature. However, the reaction rate increases by more than a factor of 5. Model predictions are again in good agreement with data, and

an Arrhenius plot yields an activation energy for the overall rate of 77.2 kcal/mol for the range of conditions studied here. This activation energy is much larger than the 40 kcal/mol [36] found in the explosive regime over a similar temperature range but at atmospheric pressure. The noted disparity of experimental and numerical results at 1068 K at large extents of reaction points to a small remaining uncertainty in the ratio for k_1/k_9 (which strongly affects the transition to explosive kinetics).

The effects of varying the equivalence ratio on the overall oxidation rate were studied at 1040 K (Fig. 5). At pressures of 1 and 3.46 atm, oxygen addition had no effect on the initial oxidation rate. The independence of oxygen concentration at 1 atm was also recently reported by Yetter et al. [8]. At 2.45 atm, oxygen addition shifts the explosive condition to lower pressures so that the oxidation rate is reduced. Experiments varying the equivalence ratio from 0.33 to 2.1 (P = 6.5 atm, T_{in} = 1040 K, initial CO of 1.0%) indicate that O_2 accelerates the oxidation in the nonexplosive regime according to $[O_2]^{1/4}$. This oxygen dependency is consistent with global kinetic studies of Dryer and Glassman [36] in the explosive regime at 1 atm and at temperatures above 1040 K. Thus, the effect of oxygen addition as a function of pressure can be complex and nonintuitive. However, the current reaction mechanism accurately predicts these trends.

The effect of varying $X(H_2O)$ on the initial oxidation rate was also studied in the nonexplosive regime (P = 6.5 atm, T_{in} = 1040 K, ϕ = 1, initial CO of 1.0%). As in the explosive regime, the rate was found to be sensitive to small quantities of H_2O. However, the accelerating effect of H_2O on the initial rate saturates at much lower water mole fractions, approximately 0.3%, in comparison to 3% in the explosive regime [4,8], in part because of increased pressure efforts on the competition of reactions (1) and (9).

Conclusions

The kinetics of moist CO oxidation have been experimentally investigated in a variable pressure flow reactor at pressures ranging from 1 to 9.6 atm, temperatures from 960 to 1200 K, and equivalence ratios from 2.1 to 0.33. Over this temperature range, the reaction dynamics of HO_2 and H_2O_2 have considerable uncertainty, and the elementary rates can exhibit significant non-Arrhenius behavior. There are no prior kinetics systems observations in the literature against which to validate HO_2/H_2O_2 mechanistic behavior over this range of conditions. By increasing the pressure above the second explosion limit in this temperature range, we have obtained such mechanistic data by studying moist CO oxidation. Similar conditions are of direct relevance to combustion and emissions chemistry of energy conversion systems. These data were used in combination with prior flow reactor, shock tube, and static reactor data to revise our previously published comprehensive mechanism. Updates of the rate constants for several HO_2/H_2O_2 reactions based on new elementary kinetic rate data were necessary to achieve agreement between high-pressure experimental measurements and model predictions. The existing literature rates for reactions (22) and (23) predict that at high pressures, CO_2 formation occurs through both channels. In separate studies of high-pressure hydrogen/oxygen kinetics, the present hydrogen/oxygen submechanism produces predictions in agreement with experimental results. Thus, both the present work and recent pure hydrogen/oxygen kinetic studies [12] are self-consistent. The significant point is that literature data for the direct oxidation of CO are self-consistent at our conditions.

Acknowledgments

The support of the U.S. Department of Energy, Office of Basic Energy Sciences through Grant No. DE-FG02-86ER-13503, is gratefully acknowledged. The authors thank Dr. J. F. Roesler for helpful discussions and Dr. J. Troe for his personal communication on HO_2 rate constant measurements. Mr. P. Michniewicz and Mrs. Y. S. Stein are acknowledged for assistance in performing the experiments.

REFERENCES

1. Hippler, J., Troe, J., and Willner, J., *J. Chem. Phys.* 93:1755 (1990).
2. Lightfoot, P. D., Vegret, B., and Lesclauz, R., *Chem. Phys. Lett.* 1:120 (1988).
3. Hippler, J., and Troe, J., *Chem. Phys. Lett.* 192:333 (1992).
4. Yetter, R. A., Dryer, F. L., and Rabitz, H., *Combust. Sci. Technol.* 79:97 (1991).
5. Dixon-Lewis, G., and Williams, D. J., in *Comprehensive Chemical Kinetics* (C. H. Bamford and C. F. Tipper, Eds.), Elsevier, Amsterdam, 1991, Vol. 17, pp. 1–248.
6. Hoare, D. E., and Walsh, A. D., *Trans. Faraday Soc.* 50:37 (1953).
7. Griffiths, J. F., and Sykes, A. F., *J. Chem. Soc. Faraday Trans. I.* 85:3059 (1989).
8. Yetter, R. A., Dryer, F. L., and Rabitz, H., *Combust. Sci. Technol.* 79:129 (1991).
9. Yetter, R. A., Ilincic, N., Dryer, F. L., Allen, M., and Gatto, J., *29th JANNAF Combustion Meeting*, NASA Langley Research Center, Hampton, VA, Oct., 1992.
10. Vermeersch, M. L., Held, T. J., Stein, Y., and Dryer, F. L., *SAE Trans.* 100:162 (1991).
11. Kim, T. J., M.S.E. Thesis, Princeton University, Princeton, NJ, 1994.
12. Kim, T. J., Yetter, R. A., and Dryer, F. L., "H_2/O_2

Kinetics: High Pressure Experimental Studies and Comprehensive Mechanism Development," *Combust. Sci. Technol.*, submitted.
13. Held, T. J., Ph.D. Thesis, Princeton University, Princeton, NJ, 1993.
14. Chase, M. W., Jr., Davies, C. A., Downey, J. R., Jr., Fulrip, D. J., McDonald, R. A., and Syverud, A. N., *J. Phys. Chem. Ref. Data.*, Vol. 14, Suppl. 1 (1985).
15. Hills, A. J., and Howard, C. J. *J. Chem. Phys.* 81:4458 (1984).
16. Kee, R. J., Ripley, F. M., and Miller, J. A., *The CHEMKIN Thermodynamic Data Base*, Sandia National Laboratories, Report No. SAND 80–8003, 1987.
17. Ritter, E. R., and Bozzelli, J. W., *THERM: Thermodynamic Property Estimation for Radicals and Molecules*, New Jersey Institute of Technology, Newark, NJ, 1987.
18. Tsang, W., and Hampson, R. F., *J. Phys. Chem. Ref. Data* 15:1087 (1986).
19. Sutherland, J. W., Patterson, P. M., and Klemm, R. B., *Twenty-Third Symposium (International) on Combustion*, The Combustion Institute, Pittsburgh, 1990, p. 51.
20. Baulch, D. L., Cobos, C. J., Cox, R. A., Esser, C., Frank, P., Just, T., Kerr, J. A., Pilling, M. J., Troe, J., Walker, R. W., and Warnatz, J., *J. Phys. Chem.* 21:411 (1992).
21. Slack, M. W., *Combust. Flame* 28:357 (1973).
22. Cobos, C. J., Hippler, H., and Troe, J., *J. Phys. Chem.* 89:342 (1985).
23. Brouwer, L., Cobos, C. J., and Troe, J., *J. Chem. Phys.* 86:6171 (1987).
24. Keyser, L. F., *J. Phys. Chem.* 92:1193 (1988).
25. Troe, J., personal communication, 1993.
26. Atkinson, R., Baulch, D. L., Cox, R. A., Hampson, R. F., Jr., Kerr, J. A., and Troe, J., *J. Phys. Chem. Ref. Data* 18 (Suppl. III):881 (1989).
27. Day, M. J., Thompson, K., and Dixon-Lewis, G., *Fourteenth Symposium (International) on Combustion*, The Combustion Institute, Pittsburgh, 1973, p. 133.
28. Friswell, N. J., and Sutton, M. M., *Chem. Phys. Lett.* 15:108 (1972).
29. Peeters, J., and Mahnen, G., *Fourteenth Syposium (International) on Combustion*, The Combustion Institute, Pittsburgh, 1973, p. 133.
30. Goodings, D. M., and Hayhurst, A. N., *J. Chem. Soc. Faraday Trans. II* 84:745 (1988).
31. Sridharan, U. C., Qiu, L. X., and Kaufman, F., *J. Phys. Chem.* 88:1281 (1984).
32. Gonzalez, C., Theisen, J., Schlegel, H. B., Hase, W. L., and Kaiser, E. W., *J. Phys. Chem.* 96:1767 (1992).
33. Roesler, J. F., Yetter, R. A., and Dryer, F. L., *Combust. Sci. Technol.* 95:161 (1994).
34. Brokaw, R. S., *Eleventh Symposium (International) on Combustion*, The Combustion Institute, Pittsburgh, 1967, p. 1063.
35. Yetter, R. A., and Dryer, F. L., *Twenty-Fourth Symposium (International) on Combustion*, The Combustion Institute, Pittsburgh, 1992, p. 757.
36. Dryer, F. L., and Glassman, I., *Fourteenth Symposium (International) on Combustion*, The Combustion Institute, Pittsburgh, 1973, p. 987.
37. Pirraglia, A. N., Michael, J. V., Sutherland, J. W., and Klemm, R. B., *J. Phys. Chem.* 93:282 (1989).
38. Sutherland, J. W., Michael, J. V., Pirraglia, A. N., Nesbitt, F. L., and Klemm, R. B., *Twenty-First Symposium (International) on Combustion*, The Combustion Institute, Pittsburgh, 1986, p. 929.
39. Michael, J. V., and Sutherland, J. W., *J. Phys. Chem.* 92:3853 (1988).
40. Baulch, D. L., Drysdale, D. D., Horne, D. G., and LLoyd, A. C., *Evaluated Kinetic Data for High Temperature Reactions*, Butterworths, London, 1976, Vols. 1 and 2.
41. Warnatz, J., in *Combustion Chemistry* (W. C. Gardiner, Jr., Ed.), Springer-Verlag, New York, NY, 1985.
42. Baulch, D. L., Drysdale, D. D., Duxbury, J., and Grant, S. J., *Evaluated Kinetic Data for High Temperature Reactions*, Butterworths, London, 1973, Vol. 3.
43. Atri, G. M., Baldwin, R. R., Jackson, K., and Walker, R. W., *Combust. Flame* 30:1 (1977).
44. Timonen, R. S., Ratajczak, E., Gutman, D., and Wagner, A. F., *J. Phys. Chem.* 91:5325 (1987).
45. Timonen, R. S., Ratajczak, E., and Gutman, D., *J. Phys. Chem.* 92:651 (1988).
46. Timonen, R. S., Ratajczak, E., and Gutman, D., *J. Phys. Chem.* 91:692 (1987).
47. Lutz, A. E., Kee, R. J., and Miller, J. A., *SENKIN: A Fortran Program for Predicting Homogeneous Gas Phase Kinetics with Sensitivity Analysis*, Sandia National Laboratories Report No. SAND87-8248, 1990.